GL-TR-90-0004

Observations of Stratiform Rain with 94 GHz and Ka-Band Radars

Roger Lhermitte

University of Miami
Rosenstiel School of Marine and Atmospheric Science
Division of Meteorology and Physical Oceanography
4600 Rickenbacker Causeway
Miami, Florida 33149-1098

23 May 1990

Final Report
Period Covered 10 April 1987 to 9 December 1989

GEOPHYSICS LABORATORY
AIR FORCE SYSTEMS COMMAND
UNITED STATES AIR FORCE
HANSCOM AIR FORCE BASE, MASSACHUSETTS 01731-5000

"This technical report has been reviewed and is approved for publication"

JAMES I. METCALF
Contract Manager

KENNETH M. GLOVER, Chief
Ground Based Remote Sensing Branch
Atmospheric Sciences Division

FOR THE COMMANDER

ROBERT A. McCLATCHEY, Director
Atmospheric Sciences Division

This report has been reviewed by the ESD Public Affairs Office (PA) and is releasable to the National Technical Information Service (NTIS).

Qualified requestors may obtain additional copies from the Defense Technical Information Center. All others should apply to the National Technical Information Service.

If your address has changed, or if you wish to be removed from the mailing list, or if the addressee is no longer employed by your organization, please notify GL/IMA, Hanscom AFB, MA 01731. This will assist us in maintaining a current mailing list.

Do not return copies of this report unless contractual obligations or notices on a specific document requires that it be returned.

REPORT DOCUMENTATION PAGE

Form Approved
OMB No. 0704-0188

1. AGENCY USE ONLY (Leave blank)	2. REPORT DATE	3. REPORT TYPE AND DATES COVERED
	23 May 1990	Final Report, 10 Apr.1987-9 Dec. 1989

4. TITLE AND SUBTITLE
Observation of Stratiform Rain With 94 GHz and Ka-Band Radars

5. FUNDING NUMBERS
PE: 61102F
PR 2310 TA G8 WU CA
Contract F19628-87-C-0106

6. AUTHOR(S)
Roger Lhermitte

7. PERFORMING ORGANIZATION NAME(S) AND ADDRESS(ES)
University of Miami
Rosenstiel School of Marine and Atmospheric Science
Division of Meteorology and Physical Oceanography
4600 Rickenbacker Causeway
Miami, Florida 33149-1098

8. PERFORMING ORGANIZATION REPORT NUMBER

9. SPONSORING MONITORING AGENCY NAME(S) AND ADDRESS(ES)
Geophysics Laboratory
Hanscom AFB, MA 01731-5000

Contract Manager: James Metcalf/LYR

10. SPONSORING / MONITORING AGENCY REPORT NUMBER
GL-TR-90-0004

11. SUPPLEMENTARY NOTES

12a. DISTRIBUTION / AVAILABILITY STATEMENT
Approved for public release; distribution unlimited

12b. DISTRIBUTION CODE

13. ABSTRACT (Maximum 200 words)

The project is concerned with observations of stratiform rain at vertical incidence conducted with a 3-mm wavelength Doppler radar and their analysis and interpretation. The data interpretation is dominated by the need to involve Mie scattering functions which exhibit deep oscillations in the raindrop size range.

These considerations lead to a method for separating the contributions of raindrops' terminal velocity and air velocity in Doppler spectra obtained from observation of rain at vertical incidence. Measurements of both weak down-updrafts and raindrop size distribution are thus possible in stratiform rain. The change of radar reflectivity and particle vertical velocity through the layer in which snowflkes are melting on their way to becoming raindrops (melting layer) is also analyzed and interpreted.

14. SUBJECT TERMS	15. NUMBER OF PAGES
Millimeter wave, Doppler radar, precipitation physics	38
	16. PRICE CODE

17. SECURITY CLASSIFICATION OF REPORT	18. SECURITY CLASSIFICATION OF THIS PAGE	19. SECURITY CLASSIFICATION OF ABSTRACT	20. LIMITATION OF ABSTRACT
Unclassified	Unclassified	Unclassified	SAR

1. Background

The general purpose of this research is to study the physics and dynamics of stratiform rain. Our contribution to the project was to acquire vertical profiles of Doppler velocity and signal intensity with a 94 GHz (3 mm wavelength) Doppler radar operated in a vertically pointing mode and to analyze the 94 GHz radar observations together with joint K_a radar observations and rain measurement at the ground using a raingage and a disdrometer. Using a 94 GHz Doppler radar for such a project yields a very high sensitivity on weak targets, a high spatial resolution due to the availability of a narrow beam and a short pulse width. Also, the raindrops' backscattering cross section vs size relationship at 94 GHz exhibits deep oscillations within the raindrop size range which provides a means to identify sizes in a Doppler spectrum observed at vertical incidence.

Our effort was divided into the following parts:

- Preparation of the 94 GHz radar
- Pilot experiment in May-June 1987
- Second field experiment in November-December 1987
- Data analysis and report preparation

2. 94 GHz Doppler radar

The radar and its performance during various projects was presented elsewhere [Lhermitte, 1987, 1988a]. A photograph of the radar is shown in Fig. 1 and the main characteristics of the radar when used in the GL project are the following:

- Peak power: 1.2 kW
- Receiver noise figure: 6.5 db DSB
- Minimum detectable signal: -99 dBm (-115 dBm with 3 s integration)
- Pulse width: 400 ns for the May experiment, 200 ns for the November experiment.
- Pulse repetition rate: 10 kHZ

- Two (transmit and receive) 3-foot antennae.

The radar reflectivity of precipitation or clouds, η, can be expressed, knowing the intensity, P_r, of the backscattering signal they produce, by the expression:

$$10\,log\,\eta = 10log\,P_r - 10log\,P_t + 10log\,4\pi R^2 - 10log\,h - 10log\,A_e \qquad (1)$$

where R is the target distance, P_t is the transmitter peak power, h is the pulse volume radial dimension, and A_e the antenna effective area.

With the radar characteristics above and including a 0.6 (two-way) antenna efficiency coefficient, η is given by:

$$10\,log\,\eta = P_r(dBm)\ - 23.5\ + 20log\,R \qquad (2)$$

where η is in cm^{-1} and R is in kilometers. In the case of a Rayleigh target (hydrometeors having a size much smaller than the radar wavelength and practically applicable only to cloud droplets), we have:

$$dBZ = P_r(dBm)\ + 56\ + 20\,logR \qquad (3)$$

where $dBZ = 10\,logZ$ is the reflectivity factor expressed in units familiar to radar meteorologists.

The radar is equipped with a processor delivering profiles of mean Doppler and mean signal intensity estimates simultaneously at 200 range gates spaced by 400 ns (60 m). For the November 1987 experiments, a new recording unit, capable of storing 4096 2-byte samples of the received signal (I and Q) at a selectable range gate, was also included in the radar equipment so that complete Doppler spectra could be calculated at any of the range gate positions. The data are acquired successively at 16 range gates as the range is stepped by 200 ns (30 m) intervals, thereby allowing observation of 480 m sections of Doppler spectra vertical profiles.

3. Millimeter wave scattering and absorption

At 94 GHz, scattering and absorption of millimeter wave radiation by raindrops is determined using Mie scattering functions rather than the more familiar (and simpler) Rayleigh scattering applicable to centimeter wave radiation.

This is illustrated by Fig. 2 which shows the backscattering cross section of water spheres, at both 35 GHz and 94 GHz, as a function of their diameter, D. The Mie function at 94 GHz exhibits a maximum at approximately 1.1 mm diameter and a well defined minimum at 1.57 mm. Fig.3 illustrates the difference between backscattering cross sections for ice and water at the 94 GHz frequency. Note that, while liquid water drops are stronger scatterers than ice spheres within the Rayleigh assumption, this does not hold for particles not small with respect to the radar wavelength, since, in that case, ice spheres are better scatterers than water drops of the same size.

Signal attenuation is also much more significant at millimeter waves, with both clouds and precipitation being strong absorbers. Within the Rayleigh scattering assumption (applicable to cloud droplets even at 94 GHz), signal absorption is proportional to liquid water and is controlled by the imaginary term of the water index of refraction which varies with droplet's temperature. This is illustrated by Fig. 4 which shows the 94 GHz absorption coefficient of cloud or fog (per $g\,m^{-3}$) as a function of water temperature [Lhermitte, 1986].

At 94 GHz, the Rayleigh assumption is not applicable to precipitation particles and signal attenuation by precipitation must be evaluated using the Mie functions. Theoretical attenuation coefficients computed using this method [Lhermitte, 1990] are shown in Fig. 5 together with an absorption coefficient vs rain intensity relationship proposed by Wallace [1988], as a least squares fit to his experimental data. Also shown in Fig.5 is a measurement (circled cross) based on experimental data acquired and interpreted as part of the research performed within the GL contract. These experimental data indicate that the attenuation calculated from *extinction* Mie cross sections is greater than that actually shown by measurements. This may be due to the contribution of forward scattering to the radiation propagating forward in the scattering medium. Investigations of the magnitude of this effect was beyond the scope of the present effort. However such investigations are possible using precipitation models and the Mie functions. They are recommended to provide the theoretical background needed to fully understand signal attenuation at millimeter waves.

4. Pilot experiment

Two field experiments (May-June and November-December 1987) were performed at the GL site in Sudbury, Mass. The first experiment was devoted to

building the radar shelter, testing the radar, and acquiring observations primarily for the purpose of evaluating the radar performance and the signal and data processing methods. Some observations in May were conducted with the radar moved outside and covered with a waterproof protective canvas.

The shelter was designed for housing of the radar and associated equipments in all weather conditions and was planned to be installed at a selected location near the main GL Sudbury facility in November. It was made of lumber and plywood and covered with corrugated fiberglass panels. The roof material was tested for 94 GHz radiation attenuation and it was found that, if dry, this material produces a 2-3 dB two-way attenuation which was judged acceptable. The actual use of the shelter in November showed that this building provided an adequate, waterproof, shelter in snow or rain conditions. However, in these conditions, the roof would hold water or snowflakes which would drastically increase the signal attenuation produced by that roof.

Suitable stratiform rain conditions occurred on May 15. A well defined melting level indicated by a sudden and drastic increase of mean Doppler due to melting of snowflakes as they fall through the $0°C$ isotherm was observed. The presence of a well- defined melting level suggests the absence of significant air vertical velocity, but we found that, in the rain below the melting level, some convection (50 $cm\ s^{-1}$ up-downdrafts indicated by time variability of the mean Doppler velocity discussed below) may have existed at certain times.

The data recording started at 09:36 EDT. The radar data indicated a cloud top at approximately 8 km but there was no precipitation observed at the ground. At 09:45 very sparse drops fell but the rain was very light and not measurable. The precipitation then increased steadily to reach drizzle to light rain (approximately 1 $mm\ /hr^{-1}$) conditions later. The observations lasted slightly over one hour during which more than 900 vertical profiles of mean Doppler and signal intensity were obtained.

A typical example of the profiles of mean Doppler and signal intensity is shown in Fig. 6. The layer separating dry snowflakes above and raindrops below is clearly shown in the mean Doppler (and to a lesser degree signal intensity) vertical profiles. Four successive profiles of both signal intensity and mean Doppler, taken at approximately 5s time intervals, are shown in Fig. 7. The signal intensity shown in Figs. 6 and 7 (and Fig. 8 below) is corrected for R^2 and signal attenuation estimated from the Wallace [1988] data and the rain intensity at the ground. Also, the velocity profiles are corrected for air density, ρ, using the

relationship $V(D) = V_o(D)\,(\rho/\rho_o)^x$ [Foote and DuToit,1969], where $V_0(D)$ is the drops' terminal velocity at the ground and $x = 0.45$ (see equation(4) below). Fig.7 reveals a remarkable steadiness of the vertical profiles (especially signal intensity).

The most striking feature in the data presented in Figs. 6 and 7 is indeed the drastic variation with height of the mean Doppler velocity produced by the melting of snowflakes when passing through the melting layer. There is a large increase (1.5 m/s to 4.5 m/s) of the mean Doppler in a 200 m (approximately 2.9 km to 2.7 km) vertical interval. This reflects the acceleration of precipitation particle fall speed as they evolve from an ice-crystal-snowflake nature to a raindrop shape. This is similar to what was observed much earlier with centimeter wave meteorological radars.

However, centimeter wave radars observations revealed a well- defined maximum of radar reflectivity (from which the name, 'bright band', was derived) occurring just below the $0°C$ level [Lhermitte and Atlas, 1963]. This was explained earlier by a combination of: i.) above the maximum, an increase of radar reflectivity due to the change of index of refraction from ice to water (7-8 dB at centimeter wavelengths); ii) below the maximum, a decrease of the concentration of precipitation particles due to their acceleration during melting and the reduced particle size after melting. Analysis of 'bright band' data were based on the fact that, a centimeter wavelengths the precipitation particles' radar cross section is evaluated using the Rayleigh assumption, e. g. the radar cross section always increases monotonically with particle size. Also, it was assumed that each particle retains its identity with no mutual interactions, break-up or growth when it evolves from an ice crystal-snowflake shape to its final raindrop shape. However, aggregation and break-up may occur and can appreciably modify the radar reflectivity and mean vertical velocity profiles [Lhermitte and Atlas, 1963].

The profiles in Figs. 6 and 7 exhibit the same increase of mean Doppler velocity associated with acceleration of particles due to melting, which was observed with the centimeter wave radars. There is also a local increase of radar reflectivity at the top of the melting layer attributed to the change of index of refraction from ice to liquid water. However, the decrease of signal intensity below the bright band, which was always observed in stratiform rain conditions with centimeter wave radars, does not occur. This can be seen in more detail in Fig. 8 which shows a vertically expanded presentation of the profiles shown in Fig.6.

The onset of radar reflectivity increase occurs slightly above (less than 30m) the height at which particles start to accelerate which is consistent with centimeter wave observations. However, as mentioned above, the radar reflectivity at 94 GHz does not decrease in the more actively melting region below as was observed with centimeter wave radars. Also, the reflectivity structure above the melting zone appears as a notch in the reflectivity profile. Indeed, moving down from 3800 meters, while the particles' mean Doppler keeps increasing, certainly due to particle growth by accretion, the reflectivity decreases to a minimum. The reflectivity minimum thus occurs in a region of steady growth, indicated by the downward velocity increase in the mean Doppler profile, in which, within the Rayleigh assumption, radar reflectivity should continuously increase as it is systematically observed at centimeter waves. The discrepancy may be explained considering the structure of the Mie function at 94 GHz shown in Fig. 3, which exhibits a well defined backscattering cross section minimum for ice spheres of 1.6 mm diameter. Considering the Mie functions in Fig. 3, this may imply that the particles grow roughly from a 1 mm to a 2 mm equivalent size in the region just above the melting level.

There was no available measurement of rain intensity at the radar site but, according to a relationship between mean Doppler and rain intensity proposed by Lhermitte [1990], the precipitation intensity was estimated to be a few $mm\,hr^{-1}$ (mean Doppler: $4\,m\,s^{-1}$). The probability of raindrops sizes greater than 1 to 2 mm in such weak precipitation is very small. Indeed, the 'dark band' above the melting level is always observed at 94 GHz in weak precipitation intensity and disappears only in moderate to heavy rain conditions. Fig. 9 shows the time variation of vertical profiles in the form of reflectivity contours presented in altitude-time coordinates for a time interval of approximately 3 minutes. Fig. 10 shows the mean Doppler contours during the same period of time. One sees that the reflectivity minimum is deepest between 10:28:00 and 10:29:30. The minimum fills as the precipitation intensifies as indicated by the increase of the mean Doppler to $4.5\,m\,s^{-1}$ at 10:29:00.

5. Second experiment

It was recognized that the Doppler data interpretation would be drastically improved by observing the complete Doppler spectrum. Therefore, in addition to the pulse pair processor providing signal intensity and mean Doppler profiles

at range gates spaced by 400 ns, a new unit was added for the recording of the I and Q Doppler signals at a one range gate position. As mentioned in section 2, the gate could be systematically moved in 16 steps of 200 ns (30 m), so that continuous profiles could be obtained at selected 480 m altitude intervals in the precipitation. The unit was capable of recording 4096 8-bit complex (I and Q) samples. The FFT processing needed for spectrum calculation was planned to be done off-line by a microcomputer also including programs for the analysis and interpretation of the data.

The 94 GHz radar was operated inside the shelter from November 26 to December 16. During the three weeks of radar operation, various clouds and precipitation were observed, but stratiform rain observations were obtained (1 to 20 $mm\,hr^{-1}$ rain) only on November 30 and December 11, 1987. For both days, observations at vertical incidence were conducted jointly with the GL TPQ-11 35 GHz radar and the 94 GHz Doppler radar. In addition, rain intensity and dropsize distribution measurements were continuously made by a raingage and a disdrometer installed in close proximity to the 94 GHz and 35 GHz radars.

As an example of the 30 November observations, ten successive signal intensity and mean Doppler vertical profiles, acquired with the 94 GHz Doppler radar 5 s apart, are shown in Fig. 11. Signal intensity is $1/R^2$ corrected but is not corrected for absorption.

The signal intensity profiles exhibit a remarkable time stability and a constant $7.8dB/km$ slope which is attributed to signal attenuation (two-way) when propagating in the rain region. The slope does not vary appreciably through the vertical profile below the melting, which indicates no significant evolution of the dropsize distribution from the melting level to the ground. This, together with the time stability of the profiles, indicates steady and homogeneous rain conditions between the melting level and the earth's surface.

Such data acquired in steady stratiform rain conditions provide an opportunity for accurate measurement of signal attenuation at millimeter wave and its relation to rain intensity. The most reliable rain attenuation measurement was made in an $8\,mm\,hr^{-1}$ rain and yielded a $3.8\,dB\,km^{-1}$ value which is shown by the circled cross in Fig.5. One sees that this data point agrees well with other experimental measurements made by Wallace [1988] also shown by the dashed line in Fig. 5.

Fig.11 shows that the signal intensity variation from profile to profile at constant altitude is very small (approximately less than 2 dB). Using a relationship,

determined earlier for 94 GHz radars [Lhermitte, 1990], between mean Doppler from raindrops falling at their terminal velocity and rain intensity, the maximum mean Doppler variation allowed by the observed signal intensity variation is: $15\,cm\,s^{-1}$. This does not agree with the observed mean Doppler variability at constant altitude (almost $1\,m\,s^{-1}$ peak-to-peak) which must be therefore attributed to up-downdrafts reaching approximately $\pm 50\,cm\,s^{-1}$. This shows that even generally stratiform conditions such as observed here may be associated with a certain amount of convection in the rain below the melting level.

The systematic increase of vertical velocity with increased altitude is due to the change of air density and can be used to determine the exponent in the relationship proposed by [Foote an DuToit, 1969]:

$$V(D) = V_0(D)(\rho_o/\rho_z)^x \tag{4}$$

The variation with altitude of the average mean velocity from data shown in Fig. 11 yields $x \simeq 0.45$.

Comparisons were made between the signal intensity profiles observed at 94 GHz and 35 GHz. An example of the results is shown by the three successive R^2 normalized profiles observed during the same time interval, shown in Fig.12 (94 GHz), and in Fig.13 (35 GHz). The profiles are not drastically different except at the top and above the melting layer, where the local increase of reflectivity associated with melting is slightly different (approximately 10 dB at 94 GHz and 12 dB at 35 GHz, attenuation corrected), and the fact that the 35GHz data do not exhibit the weak reflectivity minimum above the melting zone seen in the 94 GHz profiles.

The slopes of the vertical profiles at both 35 GHZ and 94 GHz are surprisingly similar. Since the attenuation coefficient at 35 GHz must be around $1.7\,dB\,km^{-1}$ (one way) [Lhermitte, 1990] for the observed $8\,mm\,hr^{-1}$ rainfall, the $7\,dB\,km^{-1}$ two-way) slope at 35 GHz must be in part due to some misalignment of the two (transmit and receive) TPQ-11 antennae. Aligning two transmitting and receiving antenna beams can be a major problem which was carefully considered for the 94 GHz radar, for which the beams are collinear within less than 0.1°.

Comparing 94 GHz and centimeter wave radar profiles may constitute a powerful tool for the monitoring of precipitation particles size and shape, on the basis of which their evolution, when falling through the melting level, from an ice crystal-snowflake complex geometry to the ultimate and simple raindrop shape

can be investigated.

A sizeable effort was applied to calculation and interpretation of Doppler spectra from I and Q signals recorded in the manner presented above. The spectra were computed from FFT programs implemented on a microcomputer. For each spectrum, a 4096 complex sample Fourier transform was performed. This was followed by spectrum smoothing done by a running filter with 8 $cm\,s^{-1}$ bandwidth, providing a smooth spectrum (approximately 20 degrees of freedom for each spectral density estimate), but still preserving an adequate frequency resolution in the 16 $m\,s^{-1}$ unambiguous Doppler velocity interval allowed by the pulse repetition rate.

An example of such spectra observed at vertical incidence on 30 November in a 8 $mm\,hr^{-1}$ rain is shown in Fig. 14. The spectrum reveals a clearly defined spectrum dip associated with the minimum of backscattering cross section seen in the Mie scattering functions in Figs. 2 and 3. Figs.15 and 16 show vertical profiles of Doppler spectra in a 450m altitude interval, displayed in the form of spectral density contours in velocity vs altitude coordinates. Although there are noticeable changes in spectrum structure and bandwidth, the spectral minimum (and its position on the velocity axis) remains remarkably well defined and stable, which indicates only a small contribution from up and downdrafts. Note that in the bottom of Fig.15 another minimum at 8.2 $m\,s^{-1}$ and another minimum at approximately 9 $m\,s^{-1}$ occur. This is due to an increase of the rain intensity there, with the dropsize distribution now extending to 3 to 4 mm sizes (see the 'theoretical' spectrum in Fig.17 below).

Doppler spectra observed at vertical incidence (such as shown in Fig. 14) can be simulated by assuming a M-P [Marshall and Palmer, 1948] dropsize distribution, $N = N_o\,exp(-\Lambda\,D)$ and a terminal velocity vs diameter, V(D), relationship for raindrops derived from the G-K [Gunn and Kinzer, 1949] experimental data. The expression [Lhermitte, 1988b, 1990]:

$$V(D) = V_o[1 - \epsilon xp(-6.8\,D^2\ - 4.88\,D)] \qquad (5)$$

is an excellent fit to the G-K data. In this equation, $V_o = 923(\rho_o/\rho_z)^{0.45}$ with ρ_o and ρ_z being the air density at the ground and at the altitude z at which $V(D)$ is expressed, respectively. Since falling raindrops exhibit some random variability of their fall velocity due to complex interactions between the drops and their environment and also the possible occurrence of air turbulence, any *mean* drop

terminal velocity expressed by the above $V(D)$ expression must be associated with a probability function simulating the drop vertical velocity instability. This effect on the spectra can be reproduced by submitting the predicted spectrum derived from the mean V(D) relationship to a running filter. This is equivalent to convolving that spectrum with a (Gaussian shape for instance) spectrum simulating the random velocity effect.

Fig. 17 shows a comparison between an observed spectrum and a theoretical spectrum based on a M-P dropsize distribution with Λ adjusted for best fit of the two maxima. Also shown is a correlation between observed and calculated spectra as a function of a velocity lag introduced to simulate the influence of mean air vertical velocity. Only the spectral components between 3 and 7.5 $m\ s^{-1}$ are used to calculate the correlation. One sees that the correlation is maximum near a zero velocity lag which indicates a very small contribution from air velocity (smaller than 5 $cm\ s^{-1}$). However, the theoretical spectrum exhibits a deeper minimum. This is attributed to the effect of the random components in the raindrop's fall speed mentioned above, which smears the observed spectrum.

As mentioned above, convolving the theoretical spectrum with a spectral function simulating the random velocity component corrects the problem. This is included in Fig.18 which now shows an excellent fit except for the discrepancy in the high velocity (large raindrop's diameter) part of the spectrum which is attributed to a departure from the exponential slope implied in the M-P dropsize distribution. More refined spectral models such as the Gamma function or log-normal spectra [Willis, 1988; Feingold and Levin, 1986] may be used to provide a spectral fit closer than that allowed by the M-P spectrum.

Fig. 19 shows another example of a comparison between theoretical and observed spectra. A random velocity correction has been applied and the minimum depth in the two functions is in good agreement. However the maximum correlation is now obtained for 40 $cm\ s^{-1}$ velocity lag, revealing the occurrence of an updraft of this magnitude. Note that measuring the position of the minimum on the velocity axis is an adequate estimate of air velocity and appears to be a better substitute for the method of spectrum lower bound proposed by Battan [1963].

The observed variability of spectral density estimates within a Doppler spectrum observed at vertical incidence in rain is greater than the statistical variability expected from the degree of smoothing applied to the data. It is thus interesting to note that a substantial volume of rain (more that 3000 m^3) ob-

served by the Doppler radar during a relatively short dwell time (a few seconds), still yields a Doppler spectrum with significant small scale 'natural' variability when expressed in 0.1-0.2 mm diameter intervals.

Dropsize spectrum measurements can be derived from 94 GHz Doppler radar observations of rain at vertical incidence [Lhermitte, 1988b; Lhermitte,1989]. Considering the above discussion, the following approach is recommended:

1. Define a M-P dropsize distribution with Λ adjusted for best fit of the two maximum amplitudes.

2. Perform a velocity lagged correlation to calculate the velocity shift attributed to air velocity (detecting the spectrum minimum velocity position may be sufficient).

3. Convolve the calculated spectrum with a gaussian spectrum simulating the random velocity component, adjusting the bandwidth for best correlation between the calculated spectrum resulting from that operation and the observed spectrum shifted by the velocity lag determined in 2.

4. Convolve the Mie backscattering cross section vs raindrops' velocity, $\sigma(V)$, function with a Gaussian spectrum having the bandwidth determined in 3.

5. Divide the observed spectrum shifted according to the velocity lag determined in 2 by the $\sigma(V)$ function determined in 4 to obtain the dropsize distribution expressed as a function V.

6. Calculate the dropsize distribution $N(D) = N(V)\,dD/dV$ using the (equation (5)) terminal velocity-size relationship.

The procedure above can be followed automatically by a computer program which, in addition to the dropsize distribution spectrum provides an estimate of vertical air motion and possibly some indication of air turbulence if it is a significant contribution to the random velocity component. An example of the results is shown in Fig. 20 where the radar derived $N(D)$ distribution is compared to that obtained with a disdrometer.

6. Evolution of spectra through the melting level

Doppler spectra were observed in the melting layer by attempting to scan the range gate at which I and Q signals were recorded. An example of the results is shown in Fig. 21. The altitude of the melting level had to be estimated at the time of the observations by interpreting the signal seen on an oscilloscope so that there was some uncertainty in locating its exact altitude. This is the reason why most of the vertical profile in Figs. 21 appears to be in the snow region above the melting level. The melting starts at 180 m above the lowest altitude (420m) covered by the range gate scanning and thus does not cover the total melting level depth (250m), but is sufficient to determine the Doppler spectrum evolution through it. The data show a steady evolution of the spectra with greater vertical velocity variation for the larger size edge of the spectra.

7. Conclusion

This report presents new data acquired in stratiform rain using a millimeter wave Doppler radar. Most of the effort was applied to conducting the field experiments which have generated a decent amount of data considering the limited opportunity for stratiform precipitation observations allowed by weather conditions. The raingage, the disdrometer and the TPQ-11 radar were very valuable additions to the the project.

The 3-mm wavelength radar offers the unique opportunity to 'label' particle size from the well-defined backscattering vs diameter oscillations occurring well within the raindrops' size spectrum range. Indeed, in stratiform rain conditions the occurrence of very small air vertical velocity contributions can be observed, and when the contribution from vertical air velocity is determined, reliable dropsize distribution estimates can be made. In more convective weather, measurements of up-downdrafts may be derived from the data.

More extensive observations of stratiform rain conditions in various meteorological situations, based on vertically pointing 94 GHz Doppler radar observations assisted by K_a-band and S-band radars and ground-based dropsize distribution and rain intensity measurements are needed. This would ultimately provide a better understanding of stratiform precipitation processes, such as the influence of snowflakes melting on the dynamics and physics of the rain below.

References

Battan L.,J.,1963: Some observations of vertical velocities and precipitation sizes in a thunderstorm, *Proc. 10th Weather Radar Cof.*, 303-308.

Feingold, G. and Z. Levin, 1986: The lognormal fit to raindrop spectra from frontal convective clouds in Israel, *J. Climate Appl. Metor.*, **25**, 1346-1363.

Foote G. B. and P. S. DuToit, 1969: Terminal velocity of raindrops aloft, *J. Appl. Meteor.*, **8**, 249-253.

Gunn R. and G.D. Kinzer, 1949: The terminal velocity of fall for water droplets in stagnant air, *J. Meteor.*, **6**, 243-248.

Lhermitte R. 1986: Absorption and scattering by cloud and precipitation at 94 GHz. *Airborne Doppler Radar Meeting* National Center forAtmospheric Research, Boulder Colo.

Lhermitte R.,1987: A 94 GHz Doppler radar for cloud observations, *J. Atmos. Ocean Tech.*, **4**, 36-48.

Lhermitte R. 1988a: Cloud and precipitation remote sensing at 94 GHz, *IEEE Trans. Geos. and Remote Sensing*, **26**, 207-216.

Lhermitte R., 1988b: Observation of rain at vertical incidence with a 94 GHz Doppler radar: an insight on Mie scattering, *Geophys. Res. Lett.*, **15**, 1125-1128.

Lhermitte R. 1989: Mie scattering observations by a 94 GHz Doppler radar at vertical incidence, *24th Conf. Rad. Metor.* 1-4.

Lhermitte, R. 1990: Attenuation and scattering of millimeter wavelength radiation by clouds and precipitation, *J. Oce. Tech.*.

Lhermitte R. and D. Atlas, 1963: Doppler fall speed and particle growth in stratiform precipitation, *Proc. 10th Weather Rad. Conf.*, 297-302.

Marshall, J.S. and W. McK Palmer, 1948: The distribution of raindrops with size, *J. Metor.*, **5**, 165-166.

Mie G., 1908: Beiträge zur Optik trüber Medien, speziell kolloidaller Metall-Lösungen, *Ann. Phys.*, **25**, 377-445.

Wallace, B., 1988: Millimeter-wave propagation measurements at the ballistic research laboratory, *IEEE Trans. Geos. Remote Sens.*, **26**, 253-258.

Willis, P., 1984: Functional fits to some observed drop size distributions and parameterization of rain, *J. Atmos. Sc.*, **41**, 1648-1661.

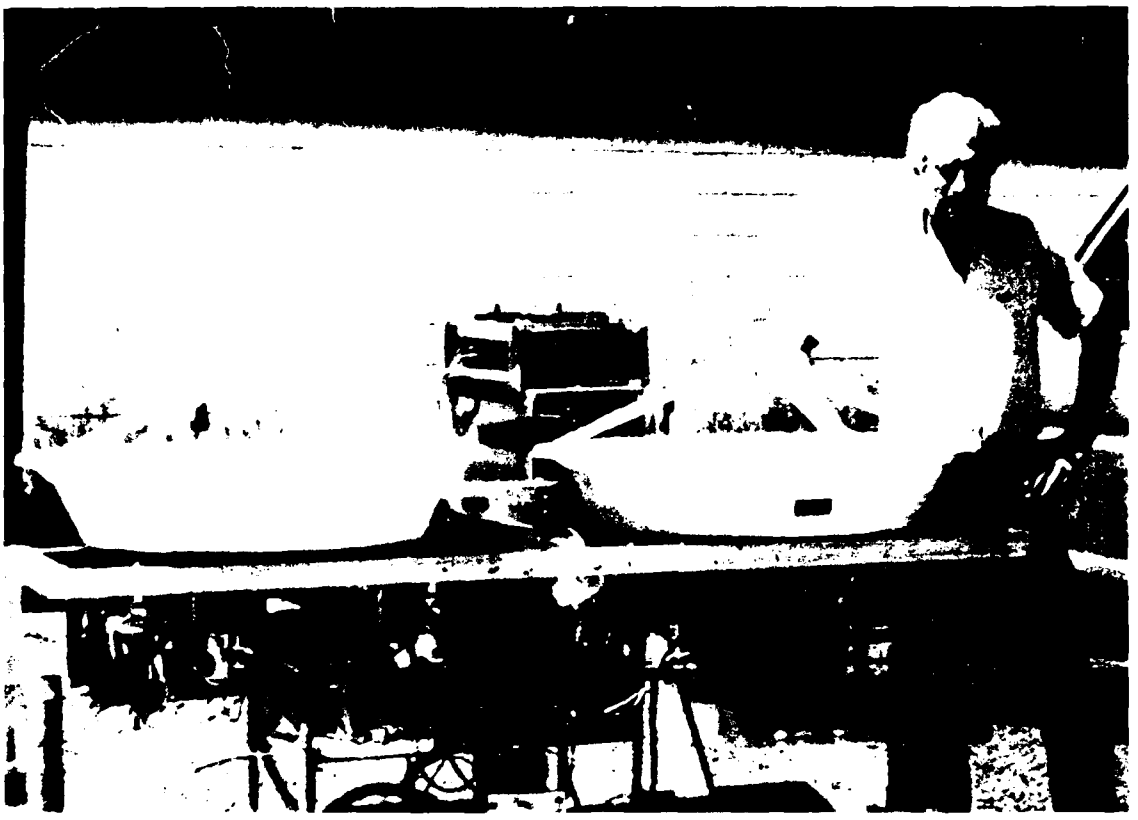

Fig. 1 Photograph of the radar

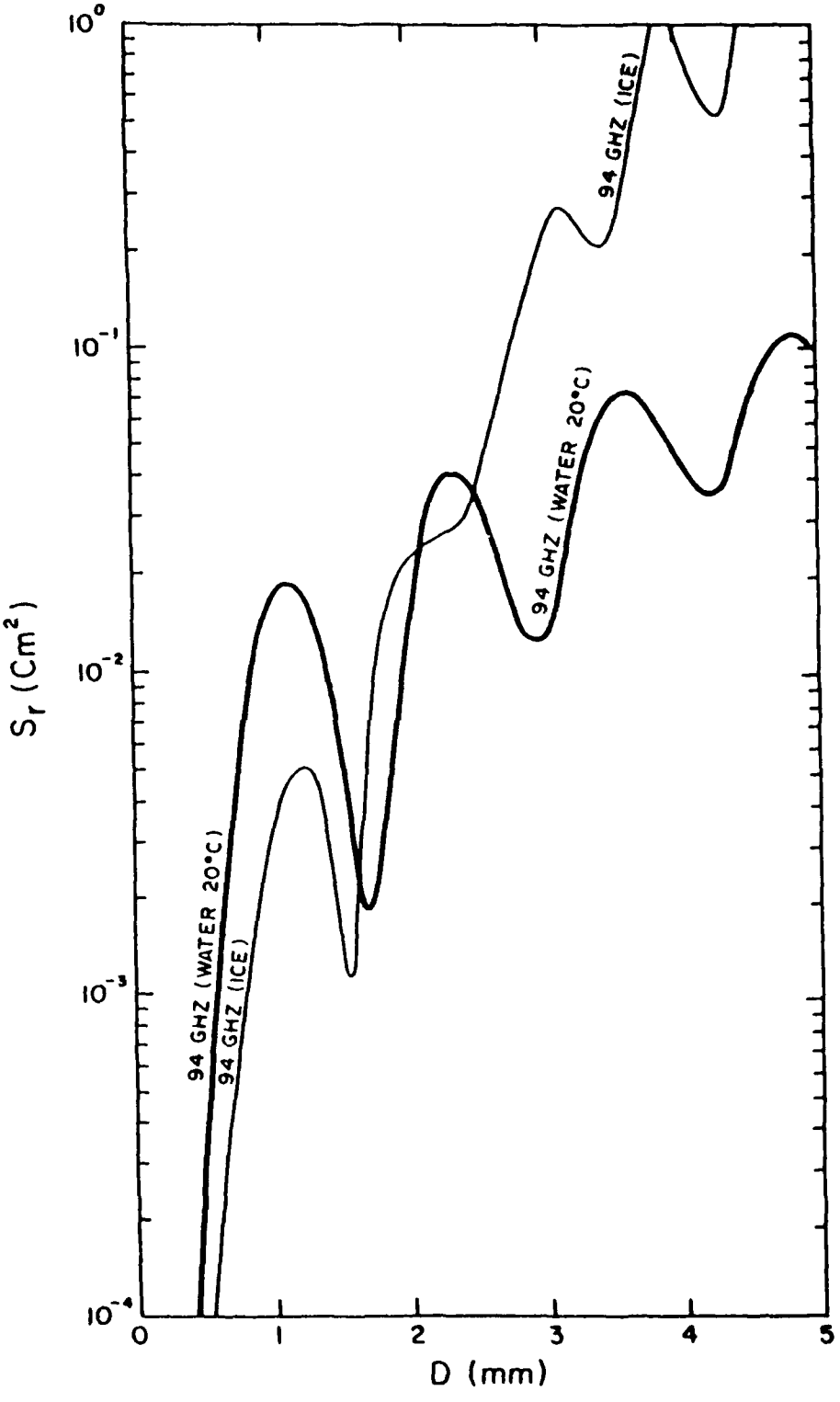

Fig.2 Radar cross secion of spherical raindrops as a function of their diameter at 35 GHz and 94 GHz. The dashed lines indicate the Rayleigh scattering approximation.

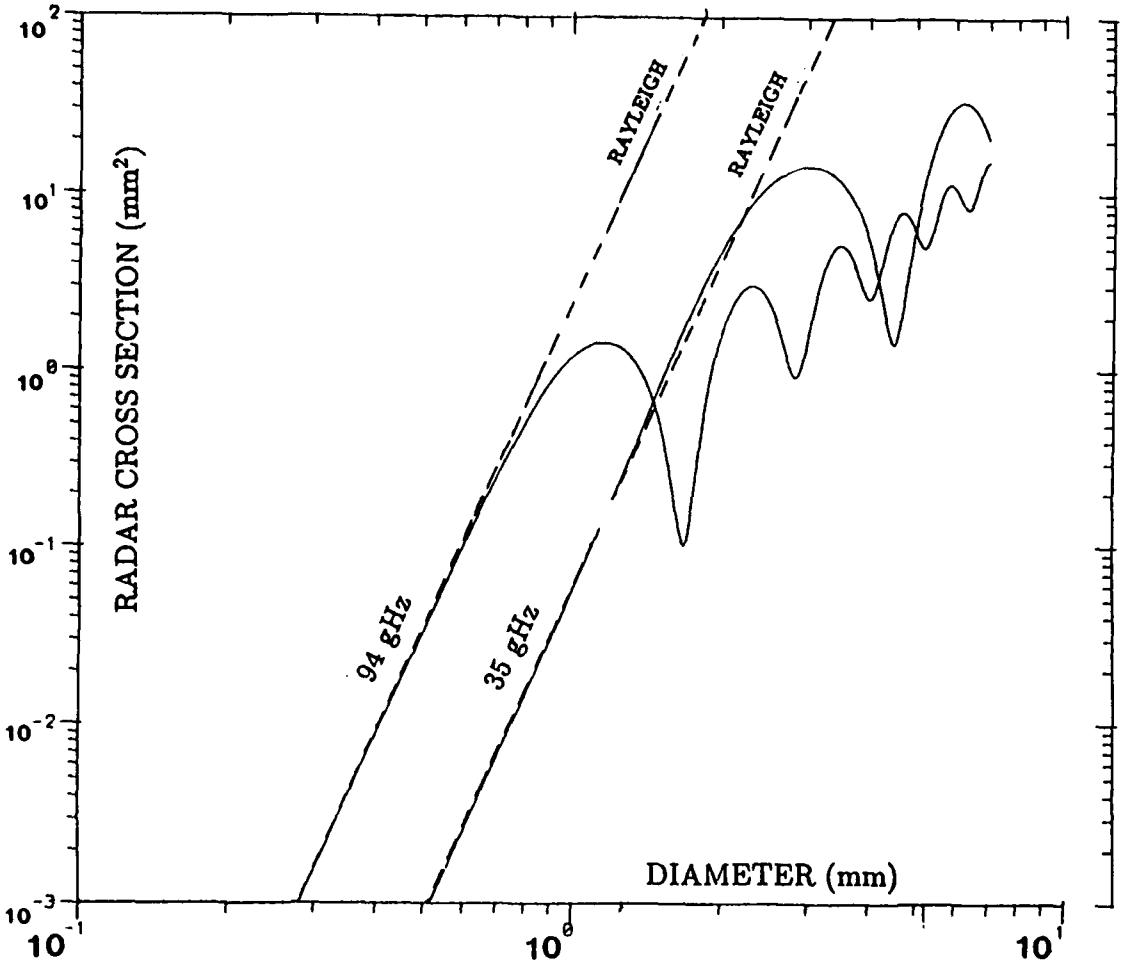

Fig.3 Backscattering cross section of water and ice spheres at 94 GHz.

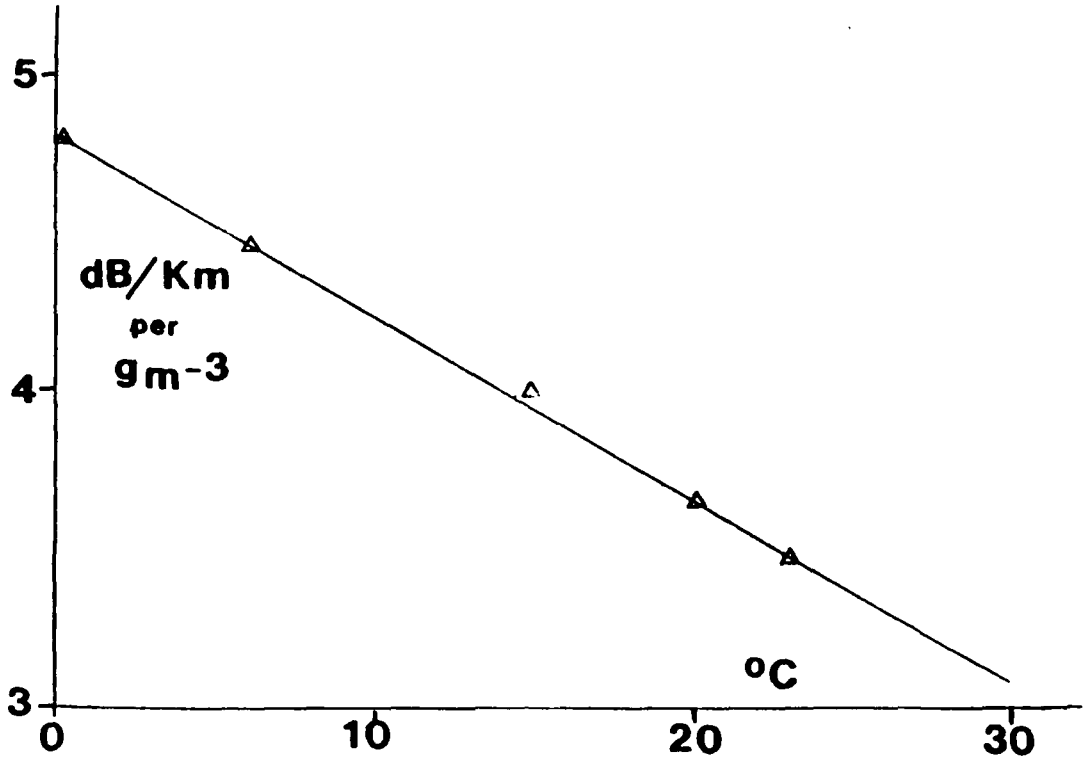

Fig.4 94 GHz absorption coefficient for liquid droplets in the Rayleigh region as a function of the droplets' temperature and normalized to liquid water content.

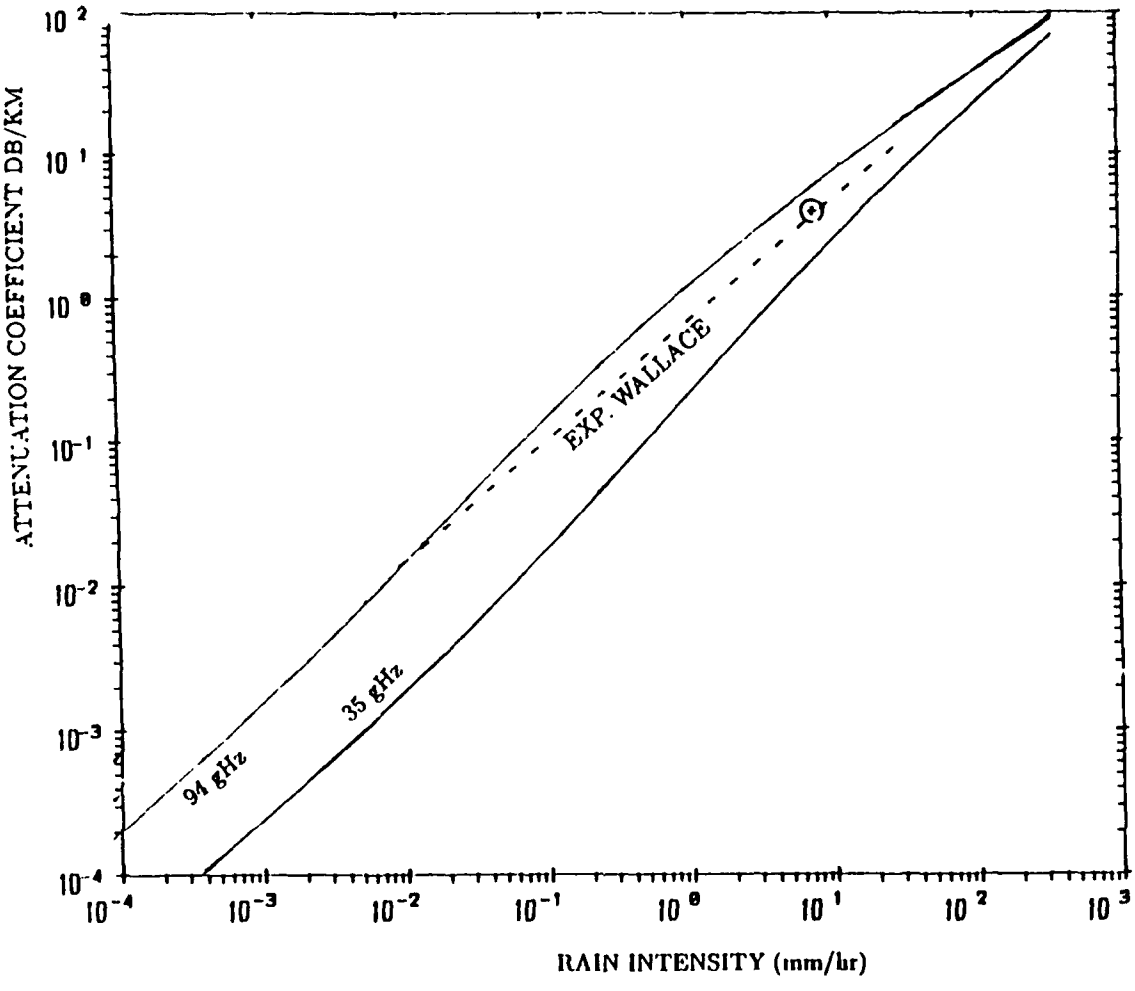

Fig. 5 Attenuation coefficient as a function of rain intensity at 35GHz and 94 GHz computed from Mie extinction cross sections. The dashed line is a least squares fit for the experimental data quoted by Wallace. The circled cross is a measurement derived from the data in this report.

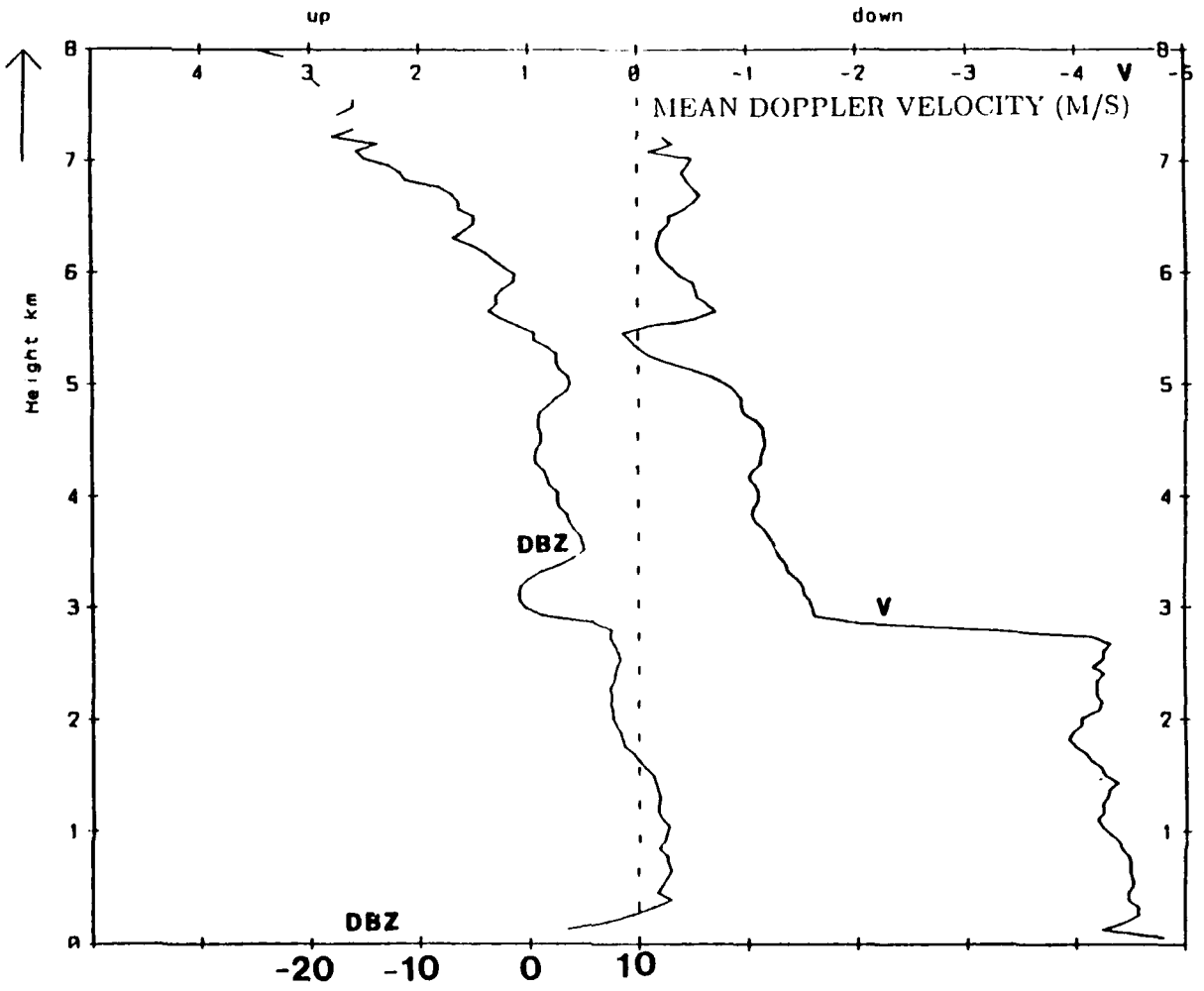

Fig.6 Vertical profiles of signal intensity (corrected for R^2 and attenuation and expressed in dBZ radar reflectivity) and mean Doppler velocity (not corrected for air density) on 15 May 1987 10:30 EDT.

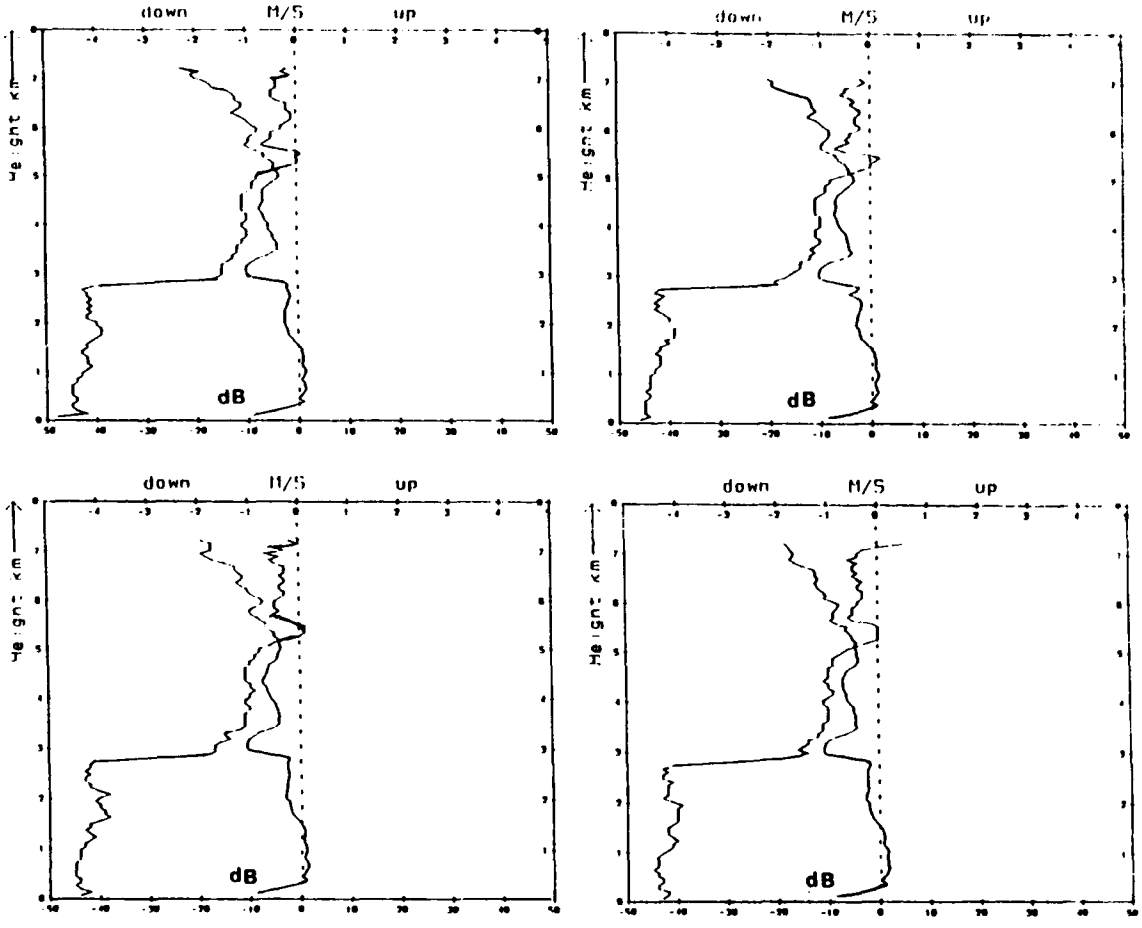

Fig.7 Profiles taken 5s apart of signal intensity and mean Doppler (not corrected for air density) on 15 May 1987, around 10:40 EDT. (signal intensity is corrected for R^2 and estimated signal attenuation. At the earth's surface, 0 dB is roughly equivalent to -10 dBZ.

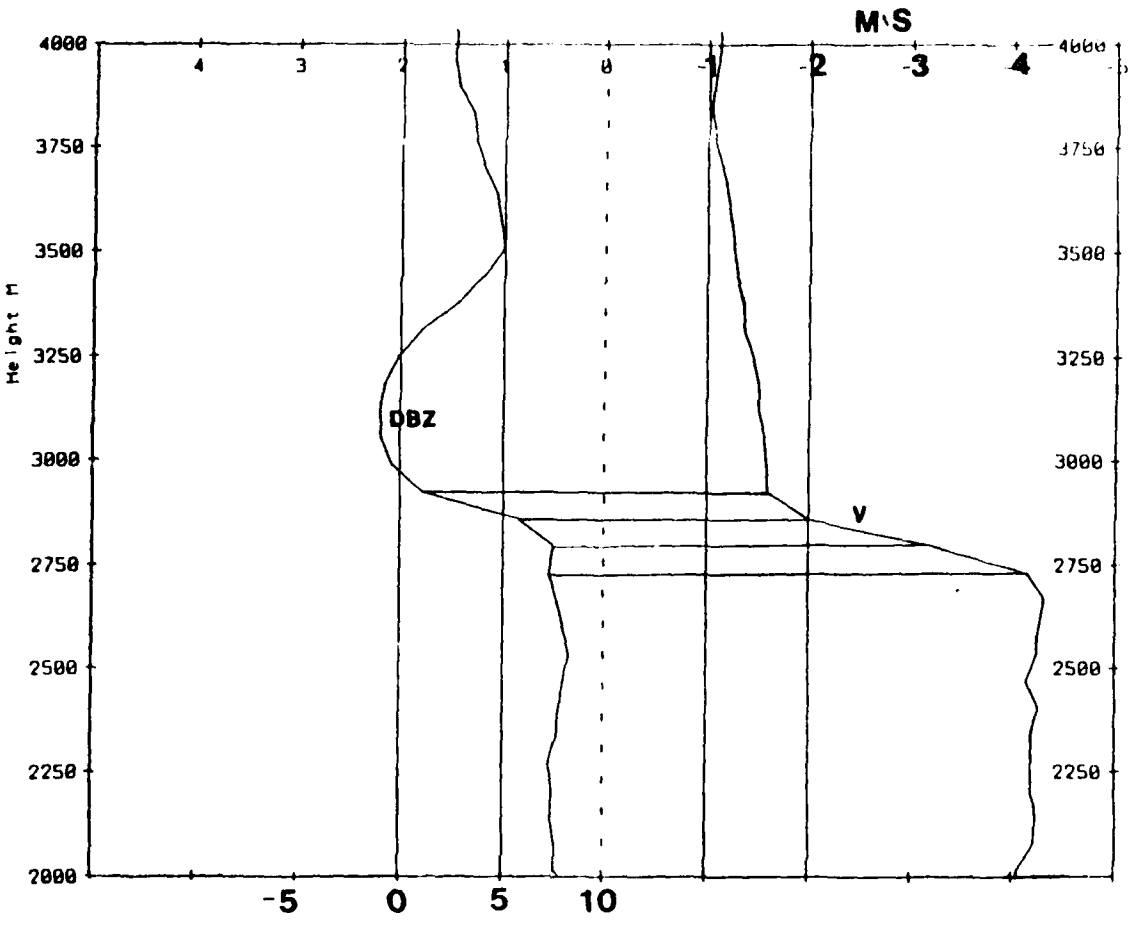

Fig.8 Same as Fig. 6 but data are plotted on a expanded scale to show the detail of the variation of radar reflectivity and mean vertical Doppler in the meiting band.

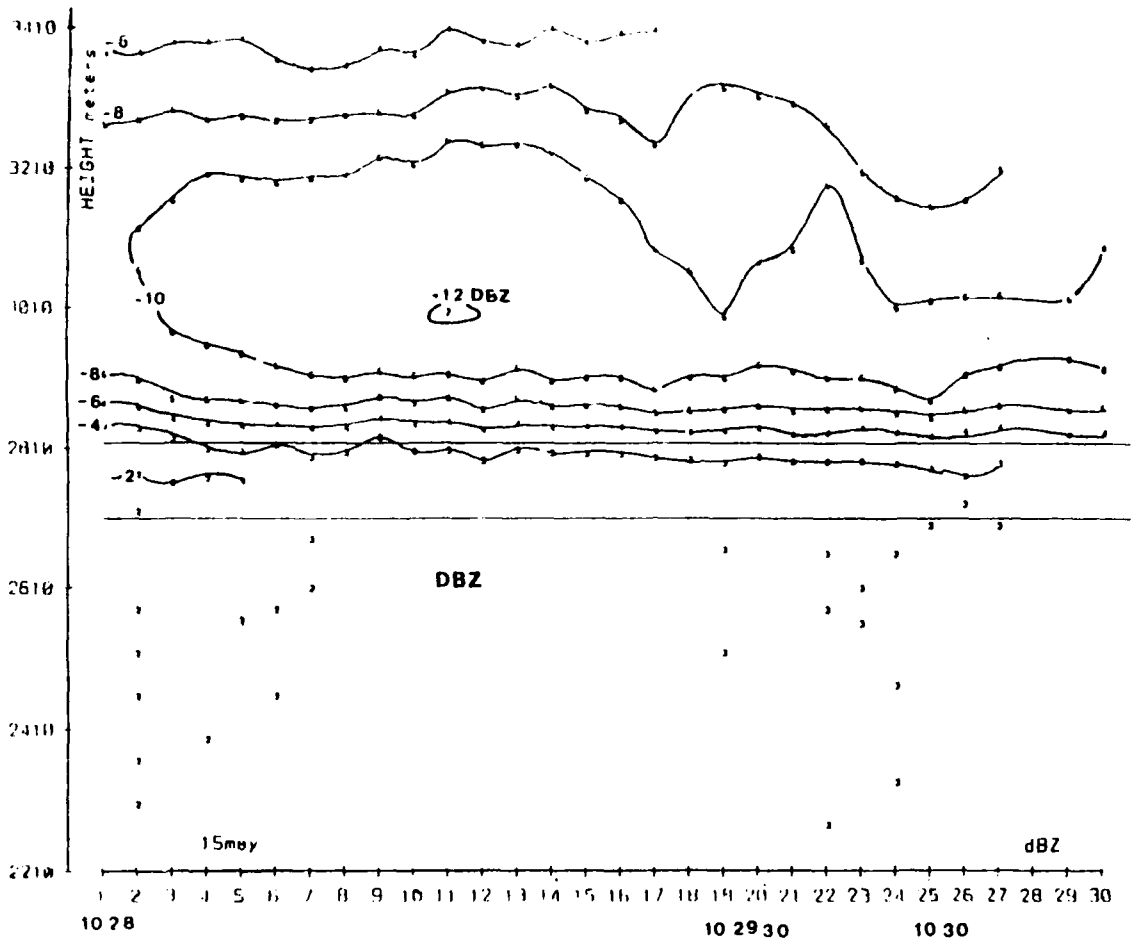

Fig. 9 Time-height display of radar reflectivity contours in the melting zone. Time starts at 10:28:00 and ends at 10:30:30, approximately. The solid line is a melting layer reference also shown in Fig. 10 for comparison between velocity and radar reflectivity data.

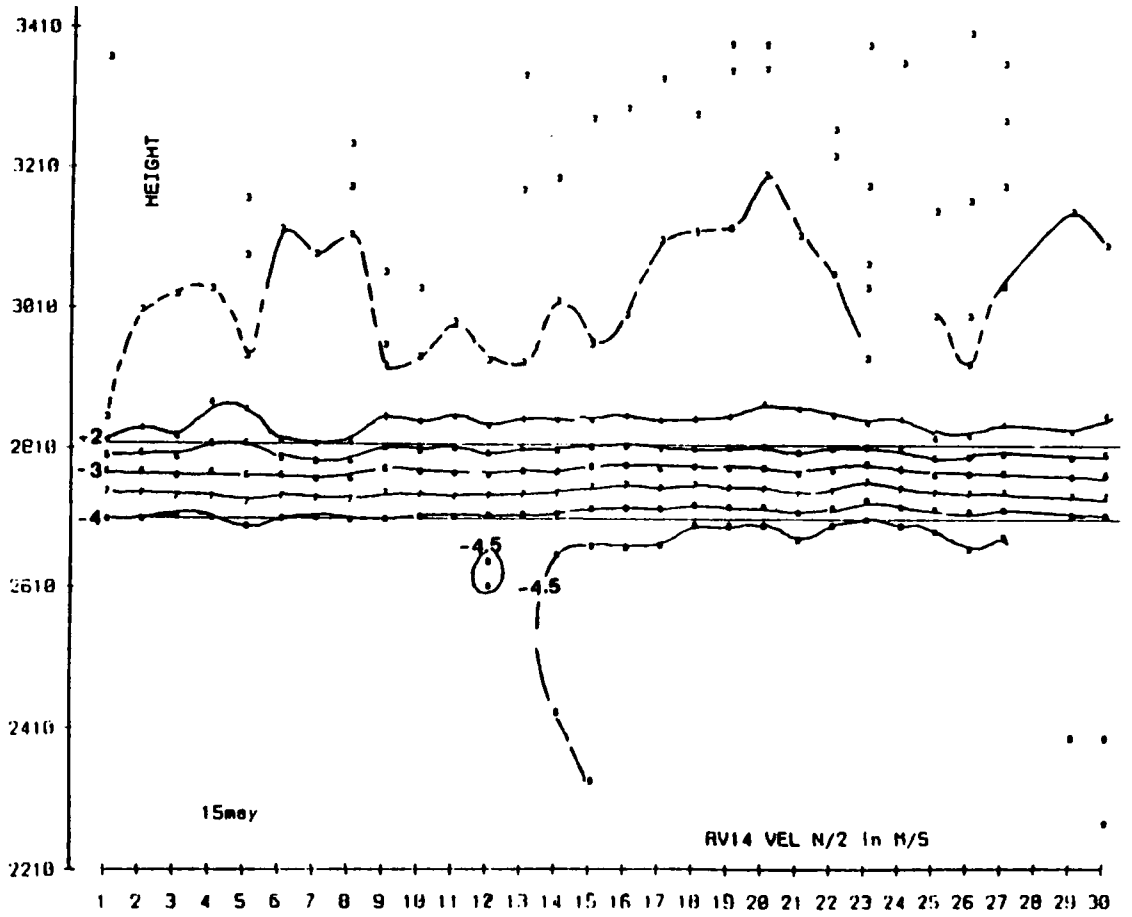

Fig. 10 Same as Fig. 9, but for the mean Doppler velocity contours at in m s^{-1}.

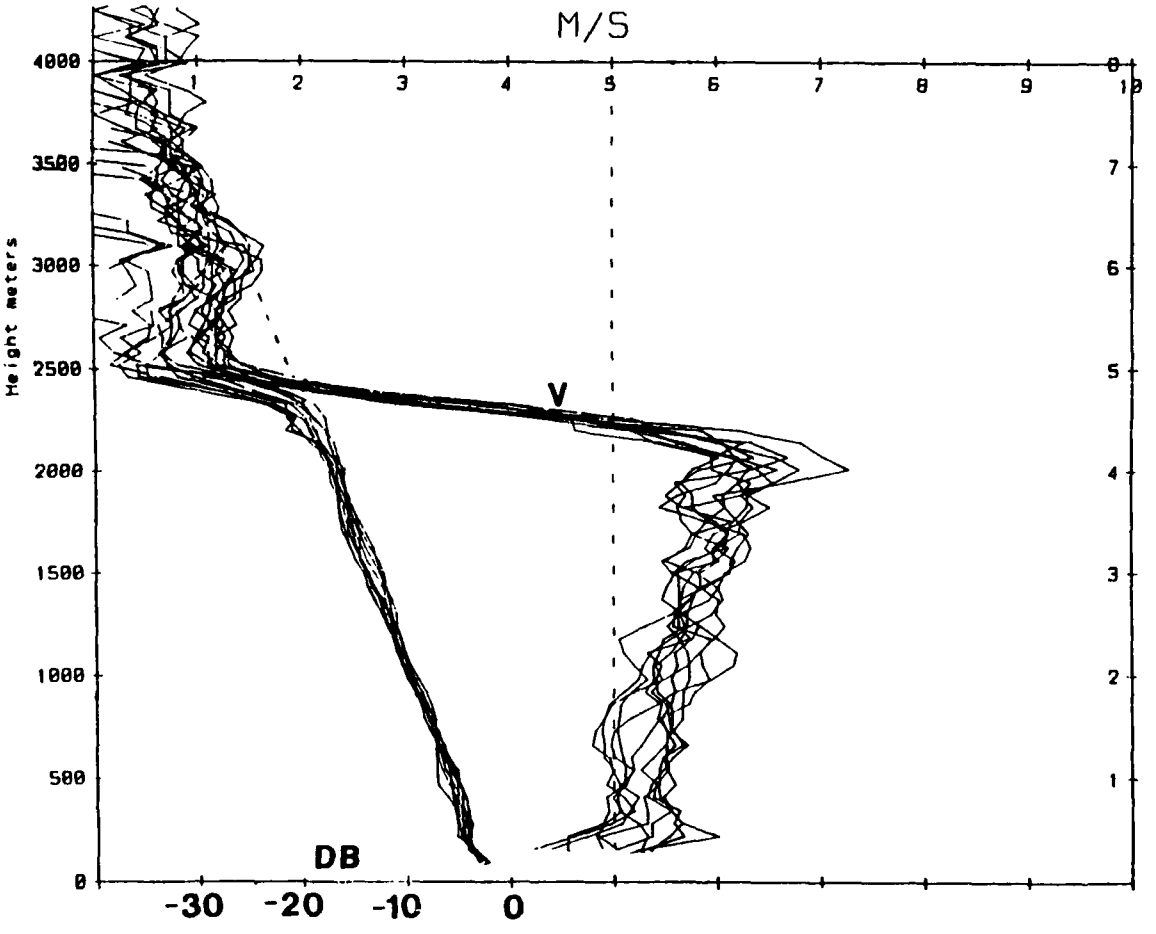

Fig.11 Presentation of 10 profiles, derived from data acquired on 30 November at 5s time intervals, of signal intensity and mean Doppler. Signal intensity is corrected for R^2 but not for attenuation and indicated in *relative* units. Note the well defined signal intensity vs height slope equivalent to $8\,dB\,km^{-1}$ two-way attenuation. Mean Doppler data are not corrected for air density.

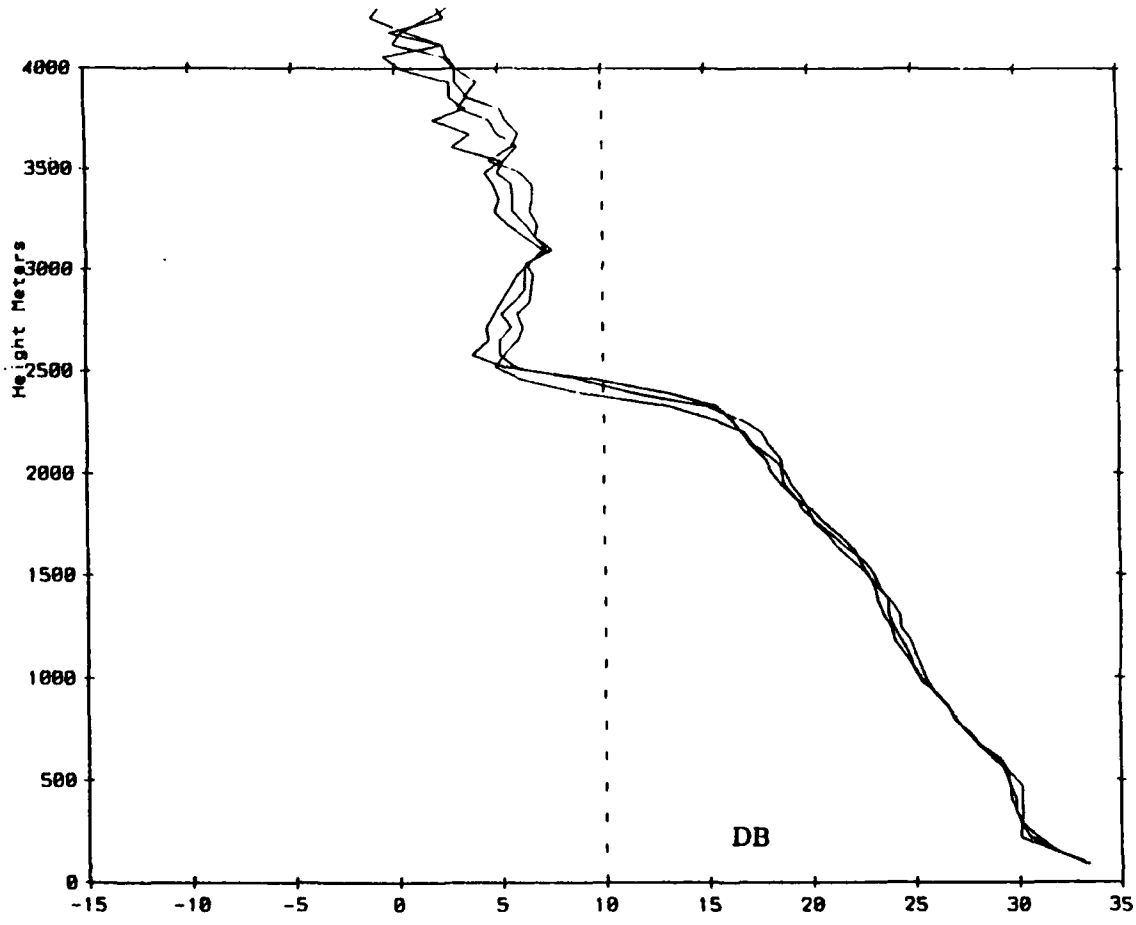

Fig. 12 R^2 corrected vertical profiles of signal intensity but not corrected for attenuation, obtained 5 s apart with the 94 GHz radar on 30 November 1987. Same data as in Fig. 11 but now shown for observations made at the same time with the TPQ-11 and shown in Fig. 13. The melting layer is slightly below 2500m.

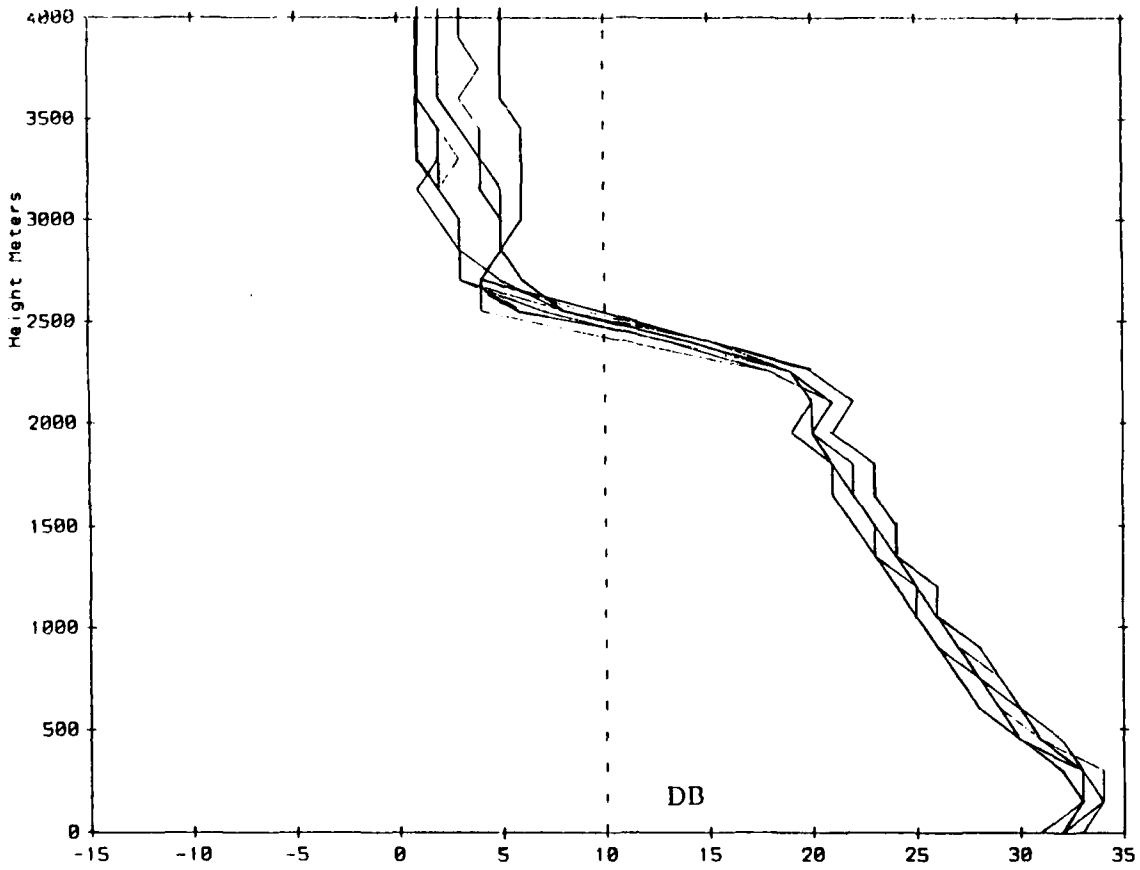

Fig. 13 Same as Fig.12 but acquired with the 35 GHz radar.

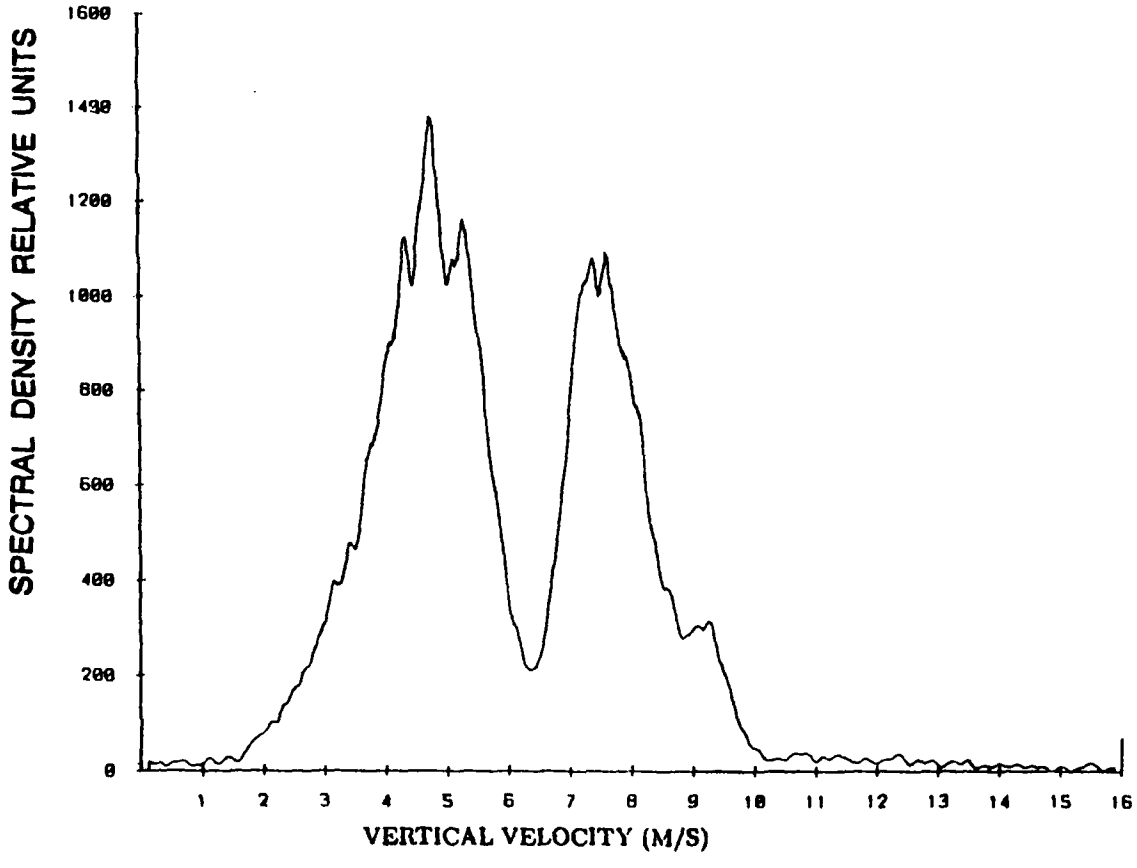

Fig. 14 Doppler spectrum obtained at vertical incidence on a $8\,mm\,hr^{-1}$ rain on November 30, 1987.

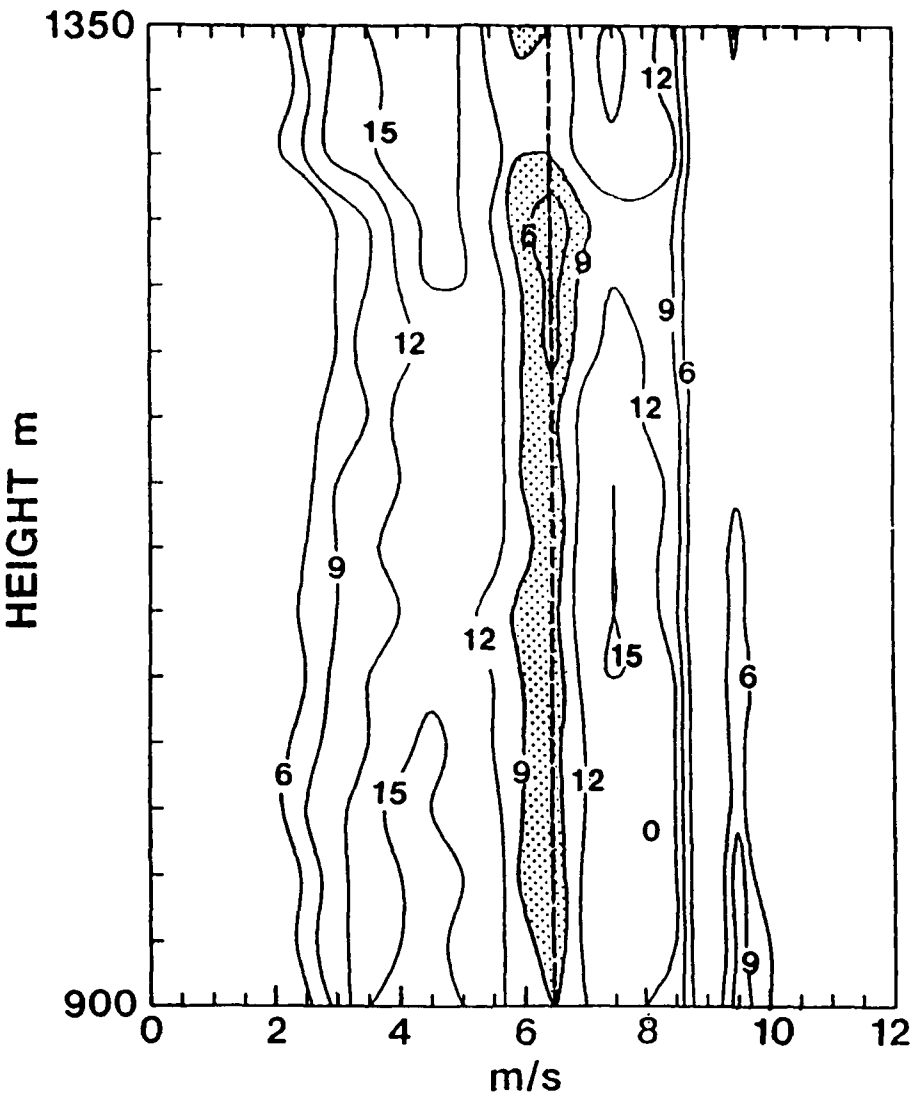

Fig.15 Variation of Doppler spectra with the altitude indicated on November 30 1987 3 dB interval contours.

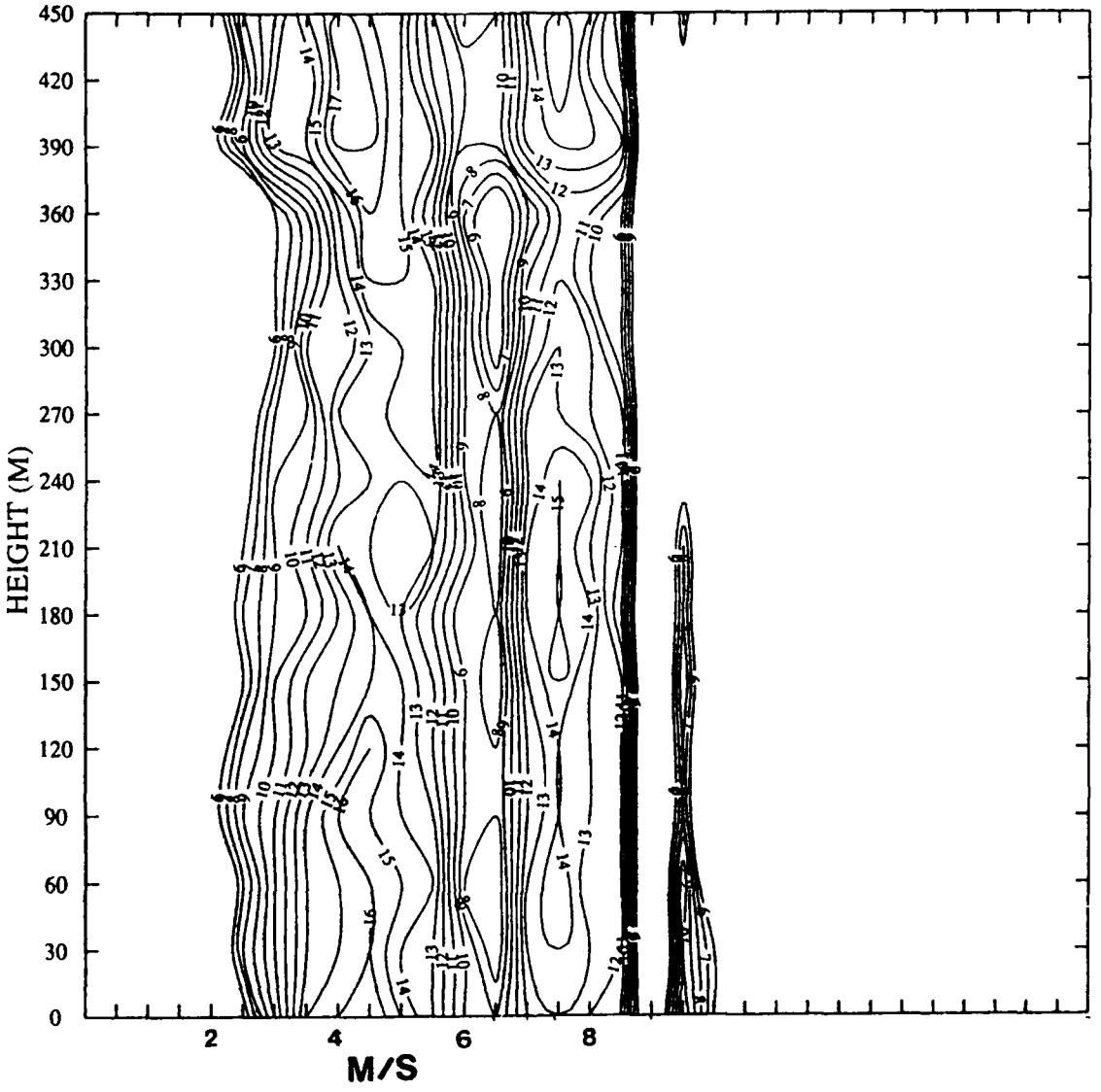

Fig.16 Same as Fig. 15 but for slightly more intense rain. 1 db interval contours.

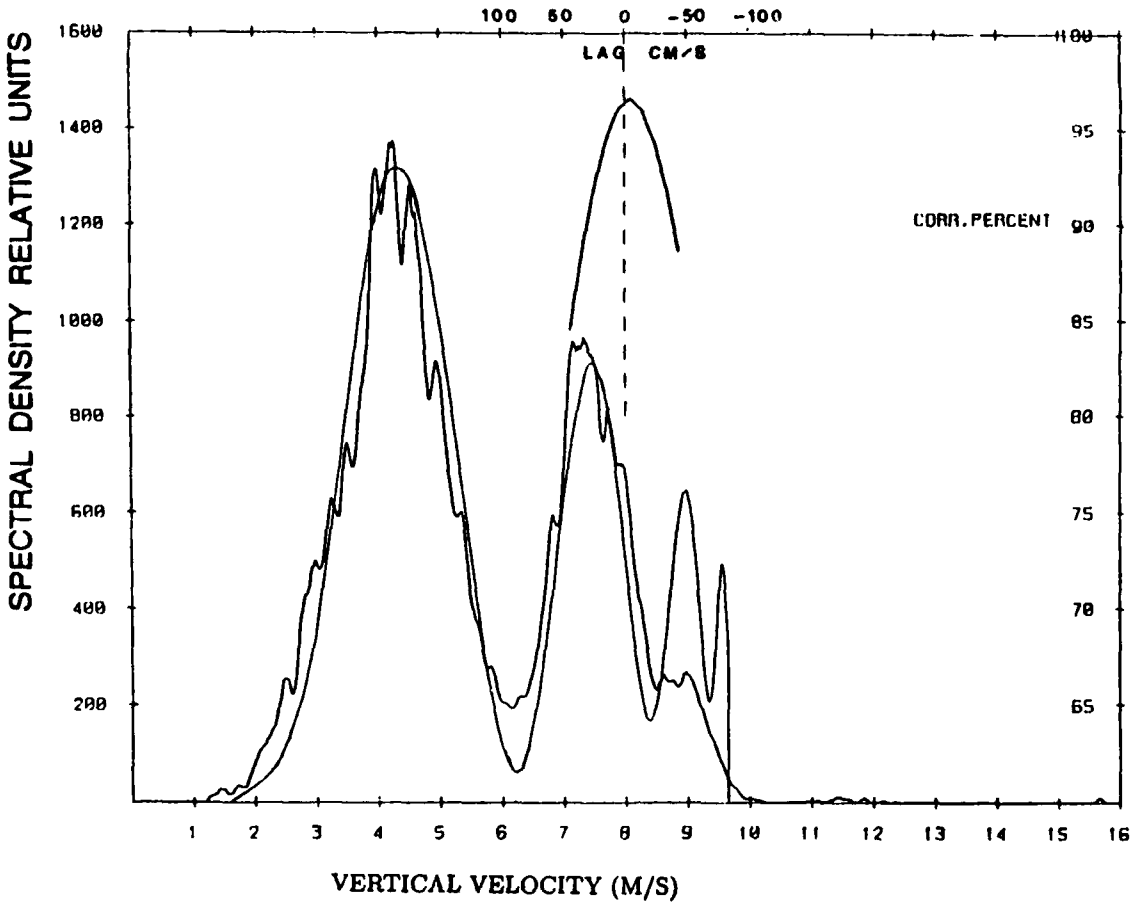

Fig.17 Doppler spectrum observed at vertical incidence together with a predicted spectrum (smooth function) based on the Mie backscattering function and a M-P dropsize distribution with Λ adjusted for the best fit of the two maxima. The function at the top of the figure is the cross correlation between the two spectra as a function of the velocity lag indicated by the top scale.

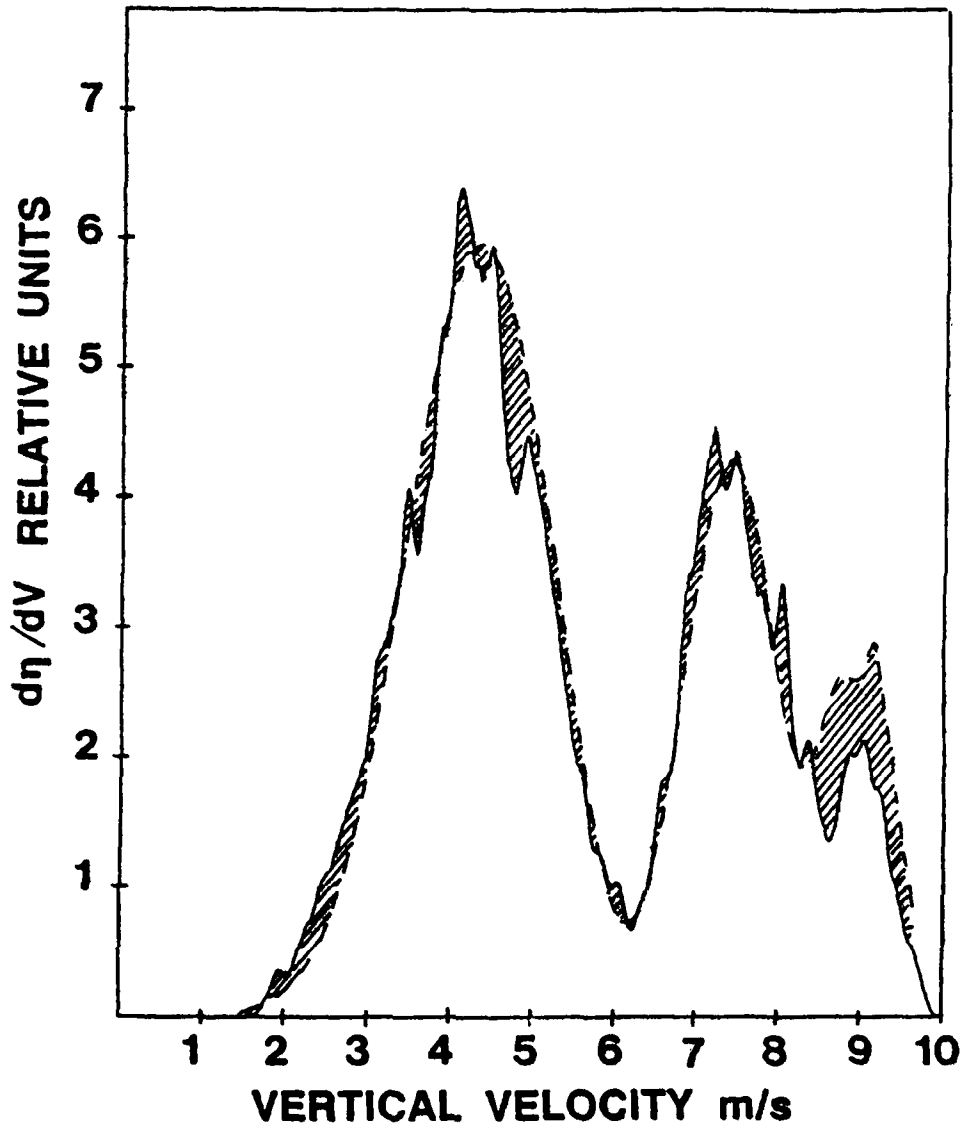

Fig.18 Example of observed and predicted spectra adjusting Λ and introducing the mean velocity and random velocity corrections (see text).

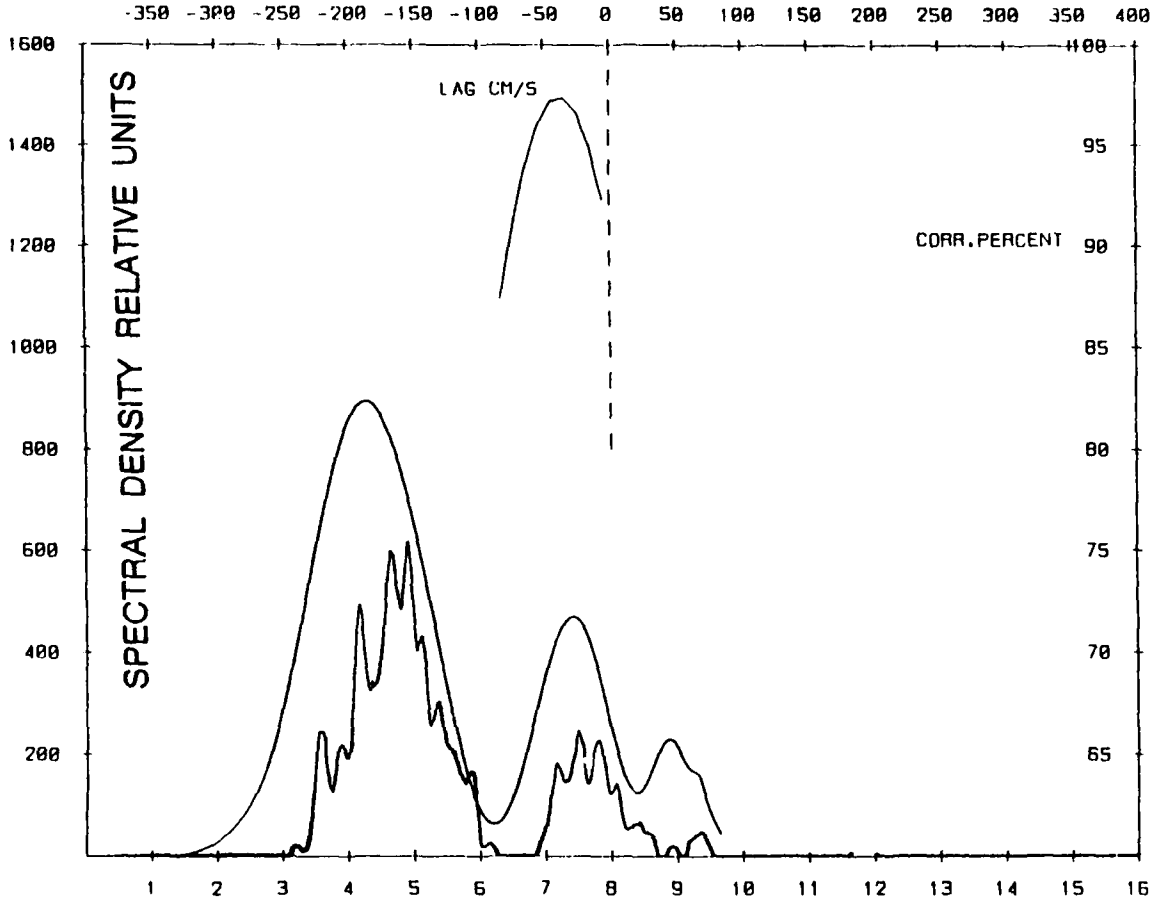

Fig.19 Example of measurement of air vertical velocity by calculation of the cross correlation between the observed and predicted spectrum.

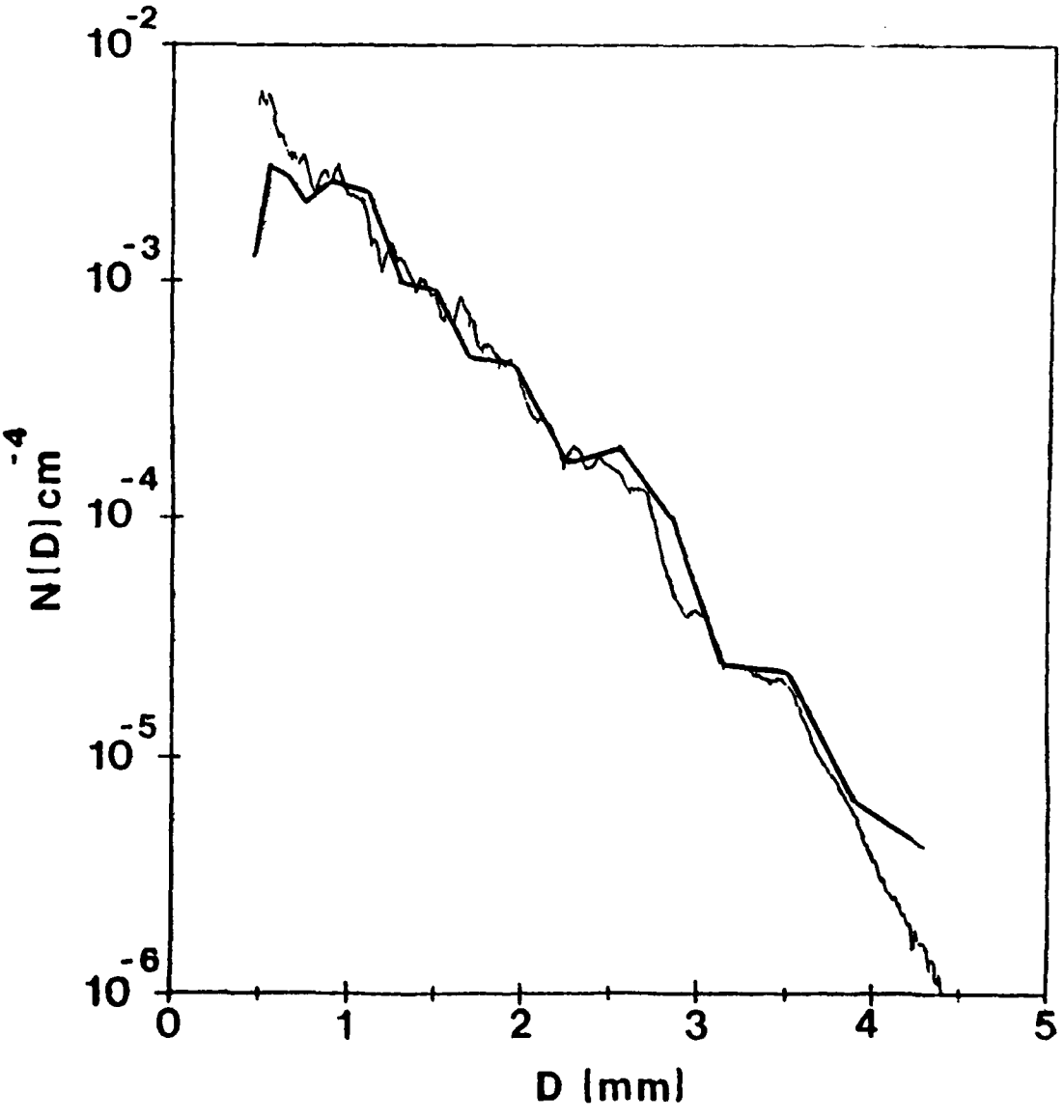

Fig. 20 Example of a dropsize distribution observed using the Doppler radar method discussed in the text and compared with disdrometer data (smoother function) acquired at the same time.

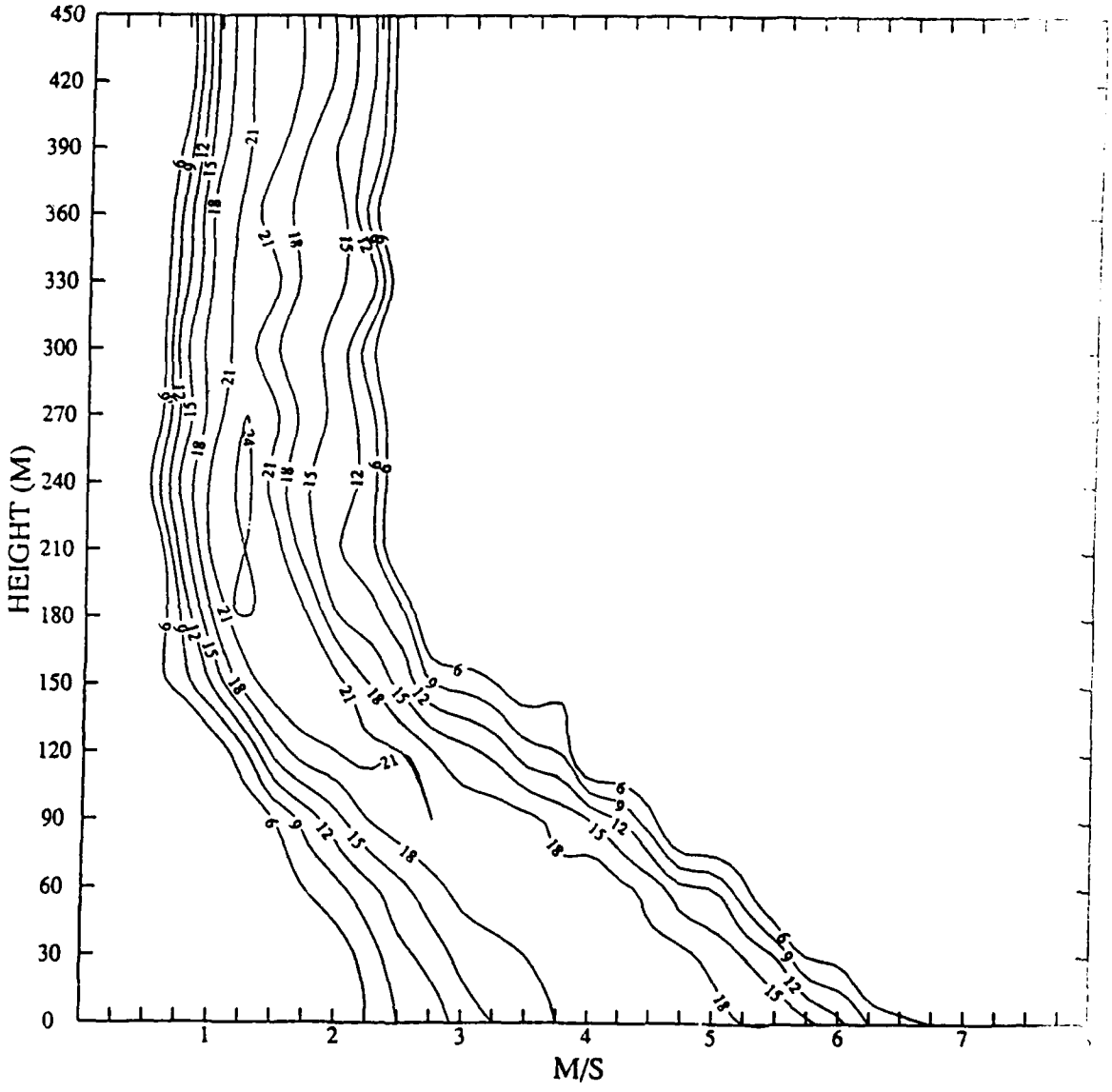

Fig. 21 Evolution of Doppler spectra in the melting layer. Contours are in dB (3 dB intervals).